ASME-ATI-UIT 2010 Conference on Thermal and Environmental Issues in Energy Systems
16 – 19 May, 2010, Sorrento, Italy

FFOWCS WILLIAMS-HAWKINGS ACOUSTIC ANALOGY FOR SIMULATION OF NACA 4-(3)(08)-03 PROPELLER NOISE IN TAKE-OFF CONDITION

Domenico Caridi*, Michele De Gennaro° and Carlo de Nicola[+]

*ANSYS UK Ltd. Sheffield (UK) S91XH, domenico.caridi@ansys.com

°Austrian Institute of Technology, Mobility Department, Giefinggasse 2, 1210 Wien, Österreich
Ph.D. student at University of Naples Federico II, Napoli (IT) 80120, michele.degennaro@unina.it

[+]University of Naples Federico II, Napoli (IT) 80120, denicola@unina.it

ABSTRACT
The use of regional turboprop aircraft, as the optimal solution for short range flights, has increased substantially in recent years. Fuel consumption and the environmental footprint are today key-issues in the aerospace industry, together with passenger comfort in terms of noise and vibration.
The goal of this paper is the evaluation of a RANS based approach for propeller noise prediction for typical aircraft take-off conditions characterized by zero free stream speed. The propeller geometry adopted for the study is the vintage NACA 4-(3)(08)-03 subsonic propeller, chosen for the wide amount of experimental data available at different rotational speeds (from 1600 to 4850 rpm) and different configurations (2-Blades and 7-Blades). The applied methodology is based on a Multiple Reference Frame RANS approach for the prediction of the steady-state load on the blades coupled with the Ffowcs Williams-Hawkings (FW-H) Acoustic Analogy, based on the Farassat & Brentner formulation of moving surfaces, for noise modelling. Optimized mesh-building guidelines and simulation strategy are provided in order to perform complete aerodynamic and aeroacoustic calculation in a time compatible with industrial design process requirements. Results of the simulation are compared with experiments showing the ability of this approach to predict noise with a discrepancy that lies in a range between 1 to 3 dB for higher rotational speeds. Investigations at lower rpm were carried out by performing an unsteady simulation as the flow field is characterized by separated flow on the blade, with a significant increase of computational time.

INTRODUCTION

Since 1995 the flight services market has increased by a significant measure in its business volume. This phenomenon is the basis of the low-cost company's success, being able to provide smart and cheap services on routes of strategic importance.

This business model is also correlated to the success of Regional Jet aircraft (i.e. A319/320/321, or B737) which are designed and optimized for 150 to 210 passengers (approximately) and for ranges between 800 and 1500 km, and are able to cover the most of the European flight market.

In particular during the last 10 years, the regional turboprop aircraft has had increasing success on short range routes (between 300 and 700 km) with smaller passenger numbers (70 seats approximately) due to an increasing demand for fast connections on routes affected by geographical barriers (i.e. sea or mountain chains). The advances in turboprop technology, which is more efficient than a turbofan for short ranges, is also proved by the success of the Bombardier Dash Q400, a new concept Turboprop aircraft designed in 2000 to provide 30% less fuel consumption and a reduced environmental footprint compared to an equivalent turbofan aircraft, which has been widely adopted by several low cost companies in Europe.

An additional key point in the modern turboprop industry is the comfort perceived by passengers in terms of vibration and noise. The great importance of acoustical performance in Turboprop industry is also proved by the Dash Q400 itself, where "Q" means "quiet".

In this paper we propose the industrial state-of-art numerical technology for simulation and prediction of propeller noise for conditions typical of take-off. Our methodology is based on a RANS aerodynamic approach for the simulation of the steady-state blade loading and acoustic sources. Aerodynamic simulations were performed with both the Multiple Reference Frame (MRF) and Sliding Mesh (SLM) approach, with the Pressure-Based Coupled Solver and k-ω SST turbulence model.

At far field microphone locations acoustic computations were performed with the Ffowcs Williams-Hawkings (FW-H) Acoustic Analogy based on the Farassat & Brentner formulation of moving surfaces.

Moreover particular attention is given to mesh generation, to build a mesh able to provide optimal y^+, an adequate number of points in the boundary layer and quality for all experimental conditions simulated.

Optimized numerical settings and strategy, including periodic rotational boundary conditions, and Full MultiGrid initialization (FMG) have also been an object of our investigation to perform accurate aerodynamic and aeroacoustic calculations with CPU time requirements compatible to the industrial design process.

The propeller geometry used for the calculations is the vintage NACA 4-(3)(08)-03 subsonic propeller, chosen for the wide amount of experimental data available in the literature at different rotational velocities as well as different blade numbers.

Calculations have been performed with the commercial software ANSYS-FLUENT.

GEOMETRY AND EXPERIMENTAL DATA SET

Experimental acoustic data published in [1], [2] have been used as reference for aerodynamic and aeroacoustic simulations. The propeller blade geometry is the NACA 4-(3)(08)-03, a straight blade propeller constructed from the NACA 16 2D airfoil section for its entire length, with a diameter of 4 feet. Geometrical details are given in Fig.1 where, Blade-Width Ratio, Blade-Thickness Ratio, Ideal Lift Coefficient and Design Angle are given as function of non dimensional span position, r/R. Geometrical data are provided from 27% to 100% of span and the blade root is assumed to be mounted on a cylindrical shaped body while the blade tip is assumed to be smooth. The blade angle is given by the reference design angle (measured at ¾ of span) added or subtracted to the β curve of FIG.1.

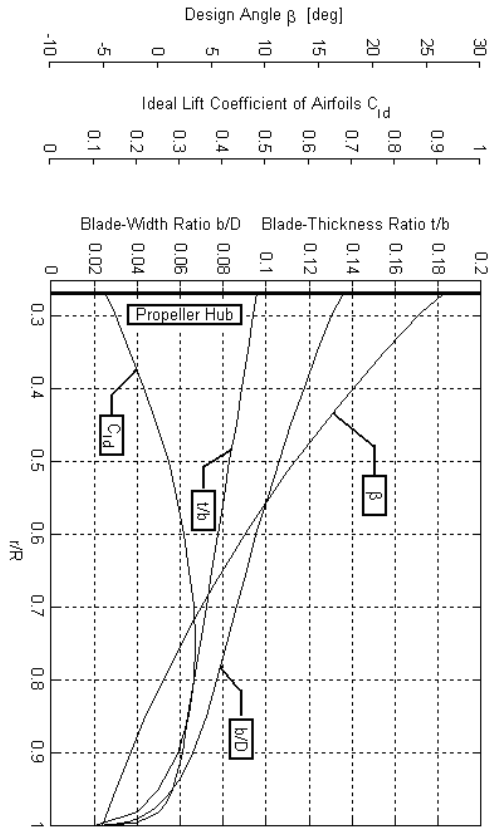

FIGURE 1. Geometry of NACA 4(3)-(08)(03) Blade

A 200 HP variable speed electric engine is used to change the rotational speed of propeller and the experiments were done with the propeller mounted on an adjustable hub which allowed the blade design angle to be changed manually. Experiments were carried out in a free-stream environment with zero wind speed. A survey rake was used to measure total pressure at a position 4 inches behind the engine, and the estimation of thrust was obtained as integration of pressure field, with an accuracy of ± 25%. Sound pressure and frequencies were measured with a Western Electric moving-coil pressure-type microphone and a Hewlett Packard Wave Analyzer. The nearest obstruction was located at 65 feet from the test stand and any discrepancy related to reflections of acoustic pressure is believed to be within the ordinary range of error of measurement for these tests. The ground is approximately located at a distance of 1 diameter from propeller axis of rotation.

A microphone was placed at ground level located 30 feet from the propeller hub and at a 15° angle behind the plane of rotation to achieve a visual angle θ = 105° (where θ is the angle from propeller axis of rotation taken from the horizontal axis in front of the propeller). This particular angular position was chosen because it is near the value of θ for *the* maximum sound pressure at the range of sound harmonics measured.

Sound pressures were measured for the first five harmonics of the fundamental rotational frequency for each test condition. Data were obtained for different rotational velocities and design angles of the propeller, and for different numbers of blades.

Experimental results show that the propeller thrust growth is different for the two and seven bladed propellers when the rotational speed is increased. It is interesting to note that for comparable thrust, the seven bladed propeller is always quieter than two bladed configuration.

NUMERICAL MODELLING

The propeller geometry was constructed from 18 airfoil sections of the NACA 16 series family. Airfoil sections were located from 30% to 90% of span with a constant spacing of 5% of span, while tip airfoil sections at 92.5%, 95%, 96.5%, 98% and 99% of span were located to follow tip chord gradient. Moreover a smooth tip was generated to cover the gap between 99% and 100% of span.

Airfoil section points were imported into ANSYS GAMBIT, where NURBS lines and surfaces were generated, and the propeller was mounted on a shaped cylindrical body used as spinner.

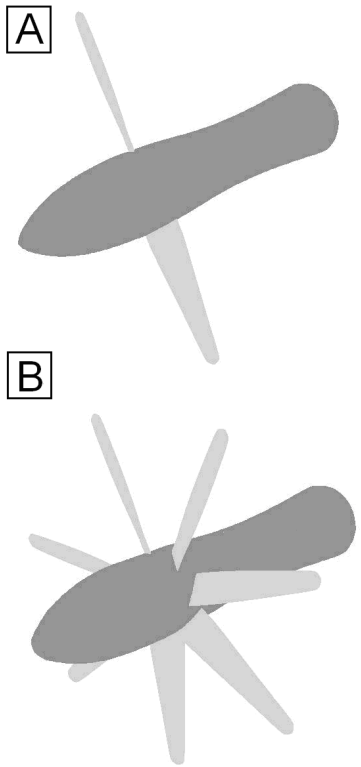

FIGURE 2. NACA 4(3)-(08)(03) Propeller
2-Bladed and 7-Bladed Configurations

The propeller tip was modelled with a smoothed rounded surface, while the propeller root was intersected with spinner, Fig.2.

In ANSYS GAMBIT a triangular surface mesh was generated, unstructured on the blade and spinner body and tri-mapped around the leading edge. A hybrid volume mesh was then generated in ANSYS TGRID with prism layer extrusion and tetrahedral mesh giving a suitable value of y^+ on the blade surface for all rotational speeds considered (in general less than 1).

Periodic sliced domains containing only one blade were generated to simulate the isolated propeller. This reduced the total number of cells as just half and one seventh of the domain had to be modelled respectively for 2 and 7 blade configurations.

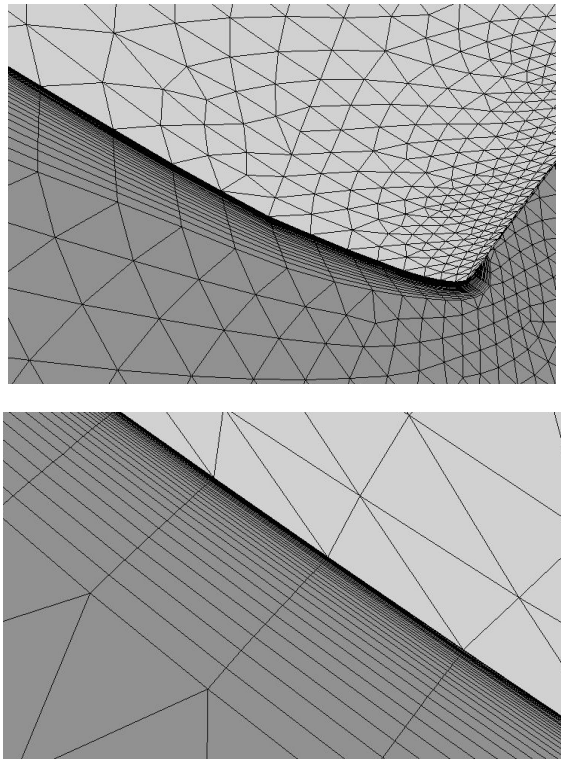

FIGURE 3. Grid Details
Leading Edge (Up) – Blade Suction Side (Down)

Prism layers were designed in order to have at least 20 layers within the physical boundary layer. This was achieved monitoring the contours of Turbulent Viscosity Ratio at different stations in the spanwise direction. By looking at those contours it is possible to estimate the boundary layer thickness by doubling the distance from the wall of the position of the maximum Turbulent Viscosity Ratio. This gave us the possibility to monitor the boundary layer thickness on the blade for both configurations and for all rpm conditions, generating a final mesh with the desired specifications.

The final grid had 40 prism layers extruded from the blade surface mesh, with tetrahedral cells filling the rest of the fluid domain, giving a total cell count of approximately 10M, per sliced periodic domain, TAB1.

Pictures of this final grid around leading edge and on the suction side are given in Fig. 3, while an example of Turbulent Viscosity Ratio contour used to detect boundary layer thickness is given in Fig. 4.

Wall optimal y^+ value for all test conditions was also a required specification. In Fig.5 a contour of the y^+ value on the blade is given for a higher rotational speed (2-Blades, 4850rpm) in order to show that for all tested cases this value is below 1 on the whole blade surface except for a small region close to tip leading edge**.**

All available experimental rpm conditions are given in TAB. 2 for configurations A and B. Lower rpm values are available for both configurations while for higher rpm they are different.

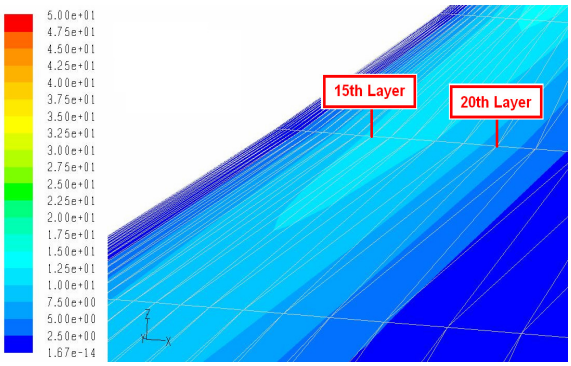

FIGURE 4. Turbulent Viscosity Ratio Contours
2-Blades – 4850 RPM – 90% of Span – Pressure Side

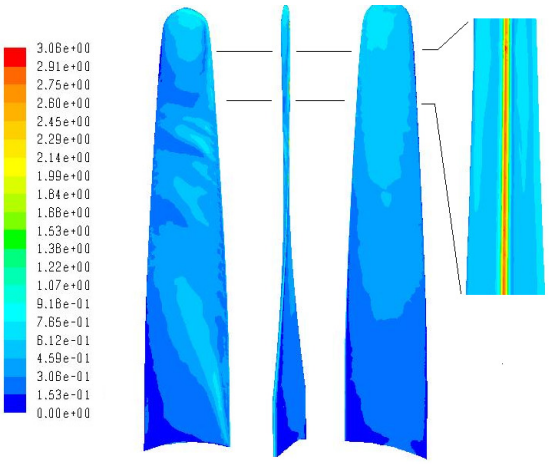

FIGURE 5. Y^+ contours on blade – 2-Blades 4850RPM
From left to right: Suction Side, Front View, Pressure Side and Tip Leading Edge Detail (Front View)

Aerodynamic simulations were performed with RANS Pressure Based Coupled Solver with Periodic Rotational Conditions, Multiple Reference Frame [5] and *k-ω* SST turbulence model (TAB. 3).

Conf. ID	Description	Cells
A	2 Blades – Periodic 40 Prisms Layers	10M
B	7 Blades – Periodic 40 Prisms Layers	10M

TABLE 1. Simulated Configurations
for NACA 4-(3)(08)-(03) Propeller

All simulations were performed at the blade angle $\beta_{3/4}$ of 16.5 deg based on experimental references.

Conf. ID	Rotational Speed [rpm]				
	1600	2680	3450	3770	4850
A	✓	✓	—	✓	✓
B	✓	✓	✓	—	—

TABLE 2. Rotational Speed Conditions for NACA 4-(3)(08)-(03) Propeller

P-V Coupling	COUPLED
Turbulence Model	*k-ω* SST
Pressure Transport Scheme	Standard
Density/Momentum/k-ε/Energy	2nd order
Asymptotic Mach Number	0
Rotational Speed	Variable

TABLE 3. ANSYS FLUENT settings

Acoustic Sound Pressure Level (SPL) at microphone locations was estimated applying FW-H Acoustic Analogy which is essentially an extension of Lighthill's equations (1) for sound pressure *p'*

$$\frac{1}{a_o^2}\frac{\partial^2 p'}{\partial t^2}-\nabla^2 p' = \frac{\partial^2 T_{i,j}}{\partial x_i \partial x_j} \tag{1}$$

to take into account noise sources related to surfaces in arbitrary motion [3,5].

The surfaces were introduced into problems multiplying the equation (1) by the Heavyside function *H(f)*, where *f=0* denotes a mathematical surface used to embed the exterior flow problem *(f>0)* in an unbounded space.

The new wave equation with the surface source terms F_i and Q_i [3,4] can be written as

$$\begin{aligned}&\frac{1}{a_o^2}\frac{\partial^2 H(f)p'}{\partial t^2}-\nabla^2[H(f)p'] = \\ &= \frac{\partial^2}{\partial x_i \partial x_j}[T_{i,j}H(f)]+\frac{\partial F_i \delta(f)}{\partial x_i}+\frac{\partial Q \delta(f)}{\partial t}\end{aligned} \tag{2}$$

and is known as the FW-H equation. It is immediately clear that if there are no surfaces (*H=1*) this reduces to equation (1).

In equation (2) the sound pressure *p'* is defined as difference of local hydrodynamic pressure and asymptotic pressure, while a_o is the asymptotic speed of sound, δ the Dirac function, and $T_{i,j}$, F_i and Q the source terms.

The first source term $T_{i,j}$ is the Lighthill's stress tensor, related to volume sources while F_i and Q_i are the FW-H source terms related to surface noise emission [5].

Without going into the detail of the formulation for each of these source terms, equation (2) is solved using the free-space Green function *G* (3), solution of the elementary wave propagation equation forced by time and space impulses (4).

$$G(x,t) = \frac{1}{4\pi a^2 r}\delta\left(t-\tau-\frac{r}{a}\right) \tag{3}$$

$$\frac{\partial^2 G}{\partial t^2}-a^2\nabla^2 G = \delta(t-\tau)\cdot\delta(x-y) \tag{4}$$

This solution is given in equation (5), where monopole, dipole and quadrupole sources terms, respectively related to body thickness, flow interaction with moving bodies and unsteady stresses, are given. It is important to notice that monopole and dipole are related to surface integrals while quadrupoles are volume sources. This contribution, often smaller than the other two, becomes zero for subsonic flows, and it is dropped off in the performed calculations [5].

$$\begin{aligned}&H(f)p'(x,t) = \\ &= \frac{1}{4\pi}\int_v \frac{\partial^2}{\partial y_i \partial y_j}\left[\frac{1}{|1-M_r|}T_{i,j}\left(y,t-\frac{r}{a}\right)\right]\frac{dy}{r}+ \quad \textit{Quadrupole} \\ &+\frac{1}{4\pi}\int_\Sigma \frac{\partial}{\partial y_i}\left[\frac{1}{|1-M_r|}F_i\left(y,t-\frac{r}{a}\right)\right]\frac{dy}{r|\nabla f|}+ \quad \textit{Dipole} \\ &+\frac{1}{4\pi a_o}\int_\Sigma \frac{\partial}{\partial t}\left[\frac{1}{|1-M_r|}Q_i\left(y,t-\frac{r}{a}\right)\right]\frac{dy}{r|\nabla f|} \quad \textit{Monopole}\end{aligned} \tag{5}$$

One of the main advantages of the FW-H model is the possibility to couple it with a steady RANS simulation for the calculation of noise sources, avoiding the need for a direct computational aeroacoustic CFD calculation. This is of particular interest for propeller applications, where for most of operating conditions, a steady load can be assumed on the blade.

Flow field initialization was done with zero wind speed, a very low rotational speed (50 rpm), and 1st order transport schemes for all variables. Then a gradual increasing of rotational velocity was applied (50→100→500→ Final rpm). At the final rpm condition, the turbulence model was switched on and after 50 iterations the transport schemes were switched to 2nd order.

The convergence of each case was checked according to thrust force and torque oscillation around the mean value (< 1%), obtaining a fully converged case in approximately 500/600 iterations.

A speed up of convergence can be achieved by initializing the flow field using a Full MultiGrid technique (FMG) [5]. This consists of building up a certain number of grid levels using the Full-Approximation (FAS) Multigrid procedure [6, 7]. The FMG algorithm performs an Inviscid Euler solution on the coarser grid level until a given order of residual reduction or a maximum number of cycles are reached. Then it interpolates the solution on the next finer level and solves, and so on up to the first grid level. This approach allowed a saving of up to 50% of computational cost achieving a fully converged solution in approximately 300 iterations.

RESULTS

Good agreement between experimental and predicted values of thrust for all simulated cases was achieved. In Fig.6 and Fig.7 comparisons between experimental and simulated data are available for the 2-bladed and 7-bladed configurations respectively.

For almost all rotational speeds simulated, CFD results are close to the upper boundary (+25%) of experimental data. No significant difference in thrust prediction between MRF and SLM simulations is obtained.

Very good agreement between experimental and simulated values of Sound Pressure Level was also achieved from 2680 to 4850 rpm for configuration A and from 2680 to 3450 for configuration B. The difference between experimental results and these cases lies in a range between 1 to 3 dB, while the under-prediction at the lowest rotational speed of 1600 rpm is quite evident.

Before discussing these discrepancies it is useful to point out the difference between the two methods used to measure the propeller noise: classic microphone-voltmeter and wave-analyzer processed data.

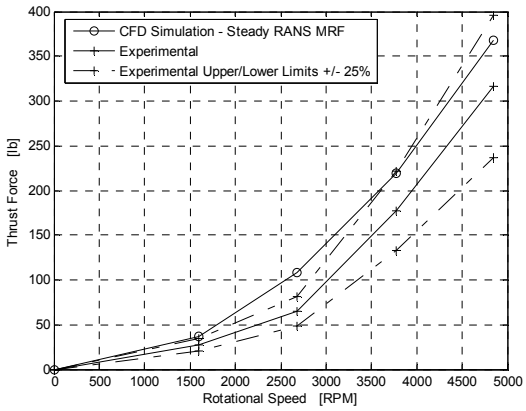

FIGURE 6. Propeller Thrust [lb]
NACA 4(3)-(08)(03) – 2-Blades Configuration

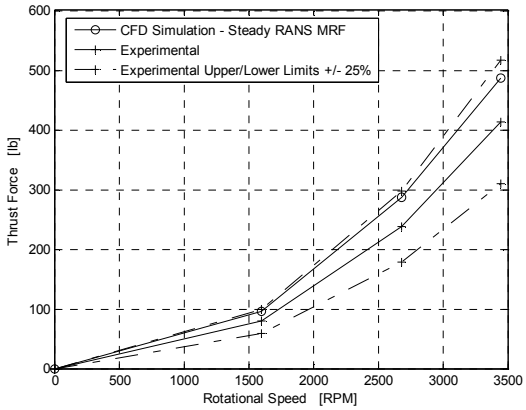

FIGURE 7. Propeller Thrust [lb]
NACA 4(3)-(08)(03) – 7-Blades Configuration

In the first case, the measured total microphone voltage is converted directly to decibels. This procedure gives the summation of the entire band of frequencies emitted. When measurements are filtered by the wave-analyzer only the sound pressure corresponding to the rotational noise-frequency peaks are summed (the first 5 harmonics).

Therefore, if the vortex noise is strong compared with the rotational noise, as is usually the case at lower rotational speeds, values determined by microphone voltmeter will be larger than values determined from wave-analyzer measurements.

Based on this and looking at the increasing discrepancies between the experimental data obtained with the two different measurement methodologies, it is evident that the noise at the 1600 rpm condition has a stronger vortex broadband noise component compared to higher rpm conditions due to the presence of separated and unsteady flow on the blade.

Moreover, this separation is also clearly visible by post-processing of the CFD results, where a wide cross flow is visible on the blade for this rotational speed.

This is also responsible for the noise discrepancy between the RANS-FWH prediction and experimental data, while it disappears for higher rotational velocities, where most of the flow is attached on the blade and the prediction is very accurate.

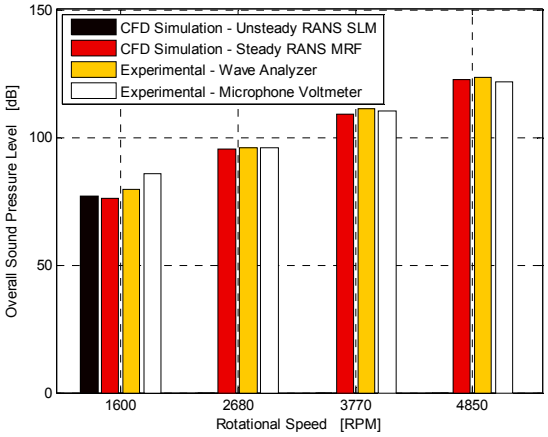

FIGURE 8. Propeller Overall SPL [dB]
NACA 4(3)-(08)(03) – 2-Blades ConFiguration

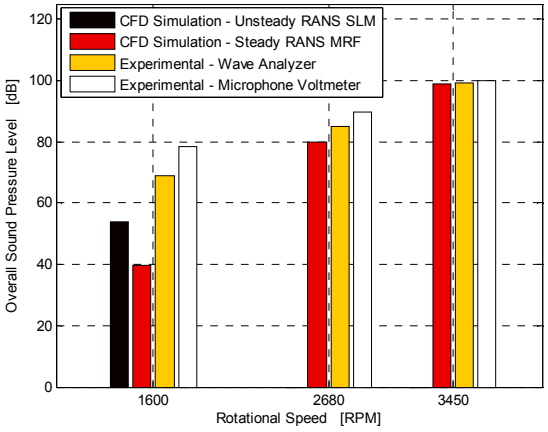

FIGURE 9. Propeller Overall SPL [dB]
NACA 4(3)-(08)(03) – 7-Blades Configuration

To better investigate this phenomenon an Unsteady RANS Sliding Mesh simulation was performed at 1600 rpm, with a time step of 0.00045 sec (1000 time steps per revolution at 1600 rpm). For each time step 15 iterations were needed to achieve a stabilizations of forces on blade, and 1 sec of simulation was performed (2000 time steps, 30000 iterations approximately).

The computational cost of this simulation was very high, due to the unsteady approach of solver, and this is the reason why only the lower rotational speed, where higher discrepancies were found, was investigated.

As we can see in Fig.8 and Fig.9 (black tab) a small correction of a few dB is given by this approach for the 2-blades configuration, while a big correction, from 42.5 dB to 54 dB, is achieved for the 7-blades configuration, but wave-analyzer is still in poor agreement at approximately 68 dB.

This results suggest us that to obtain better prediction at very low rotational speed such as 1600 rpm, more accurate simulations are needed to be able to catch all the transient features and broadband noise (DES, LES or SAS turbulence model, smaller timestep, finer hexahedral grid), with a much higher computational cost.

The possibility of reducing the computational cost of RANS-FWH, was investigated by performing some simulations on a coarser grid.

A new grid with only 5 prism layers and a 2.2M total cell count per sliced periodic domain was therefore generated. Simulations were performed with the MRF steady state approach, with RANS modelling and a wall function, and the Full MultiGrid Initialization technique (FMG) as used for the 10M cells grid. With this coarser grid a fully converged solution was obtained in approximately the same number of iterations (about 300) but with a very competitive computational time for an industrial simulation, about 3 hours on a dedicated LINUX QUAD-CORE Machine, with a 2.8GHz CPU Clock, 85% lower than finer 10M computational grid.

Simulations were performed at the higher rotational speed for both blade configurations, achieving an SPL prediction within 0.5 dB of that of the 10M cell grid.

The reason for the small difference in the noise prediction between the fine and coarse grid can be explained by the following considerations:

- According to equation (5) the FW-H model takes into account the effects of monopole and dipole sources related to surface integral of pressure loads on emitting surfaces
- Pressure loads are mostly related to blade lift and for attached flow this is mainly an inviscid problem
- At higher rotational speeds in our case the flow is attached

We can conclude that, only in the case of attached flow, a coarser gird can be used to perform an indicative analysis of propeller noise at a cruise condition. Moreover this can be important in order to save time for early design stage simulations, where computational cost and time play a fundamental role, but for off-design conditions, where flow is characterized by zones of separation, it is recommend that a more refined grid is used.

CONCLUSIONS

An extensive study has been carried out for propeller noise simulation in industrial applications.

The investigation began with aerodynamic simulations of propellers. A deep exploration into the computational methods available for simulating rotors was carried out using Multiple Reference Frame, Sliding Mesh and Periodic modeling approaches, providing a detailed description of mesh building guidelines and solver numerical settings for propeller dynamic and acoustic simulations.

A computational grid of 10M cells was generated with 40 prism layers on the blade to achieve optimal resolution of the boundary layer and an optimized simulation strategy of approximately 300 iterations has also been the subject of the study, being able to perform the aerodynamic and acoustic simulation of a NACA 4-(3)(08)-(03) propeller with time requirements compatible with an industrial design process.

The results show that RANS-MRF analysis together with FW-H Acoustic Analogy can be used to predict propeller far-field noise in take-off conditions for a NACA subsonic propeller providing very accurate results for higher rotational speeds and attached flow conditions.

Increasing discrepancy was obtained for the lower rpm condition, ascribing this effect to the transient phenomena involved in separated flows. Better agreement was obtained for this case with a highly CPU expensive URANS-SLM simulation.

Finally RANS-MRF simulations were performed on a coarser grid of 2.2M cells, giving good results for the design condition with very fast calculation times, being able to perform a complete aerodynamic and aeroacoustic simulation in less than 3 hours on a dedicated LINUX Quad-Core machine, 2.8 GHz Core Clock.

Simulations were performed with the commercial software ANSYS-FLUENT.

ACKNOWLEDGMENT

M. De Gennaro is grateful to the EC for the support for the present work, performed within the EU FP7 Marie Curie ITN project VECOM (Grant Agreement 213543).

We also thank David Mann and Florian Menter from ANSYS Ltd. for their support and suggestions.

REFERENCES

[1] NACA Technical Note 1354, Comparison of Sound Emission from Two-Blade, Four-Blade, and Seven-Blade Propeller, July 1947.

[2] NACA Research Memorandum, L50D28, Effect of Compressibility and Camber as determined from an Investigation of the NACA 4-(3)(08)-03 and 4-(5)(08)-03 Two-Blade Propellers up to forward Mach Numbers of 0.925, June 1950.

[3] K. S. Brentner and F. Farassat, An Analytical Comparison of the Acoustic Analogy and Kirchoff Formulations for Moving Surfaces, AIAA Journal, 36(8), 1998.

[4] J. E. Ffowcs-Williams and D. L. Hawkings, Sound Generation by Turbulence and Surfaces in Arbitrary Motion, Proc. Roy. Soc. London, A264:321-342, 1969.

[5] FLUENT 6.3 Full Manual, ANSYS-Fluent Inc., 2006.

[6] A. Brandt, Multi-level Adaptive Computations in Fluid Dynamics, Technical Report AIAA-79-1455, AIAA, Williamsburg, VA, 1979.

[7] A. Jameson, Solution of the Euler Equations for Two Dimensional Transonic Flow by a Multigrid Method, MAE Report 1613, Princeton University, June 1983.